JOURNAL OF SOLID STATE CHEMISTRY 105, 211–222 (1993)

Dehydration of $MoO_3 \cdot 2H_2O$: A Neutron Thermodiffractometry Study

N. BOUDJADA,*¶ J. RODRÍGUEZ-CARVAJAL,†§ M. ANNE,* AND M. FIGLARZ‡

*Laboratoire de Cristallographie, C.N.R.S., associé à l'Université J. Fourier, B.P. 166, 38042 Grenoble Cedex 09, France; †Institut Laue-Langevin, 156 X, 38042 Grenoble Cedex, France; and ‡Laboratoire de Réactivité et de Chimie des Solides, URA CNRS 1211, Université de Picardie, 33 Rue Saint Leu 80039 Amiens Cedex, France

Received October 26, 1992; accepted November 2, 1992

A neutron powder thermodiffractometric study of the dehydration reactions $MoO_3 \cdot 2H_2O \rightarrow MoO_3 \cdot H_2O \rightarrow MoO_3$ has been carried out in order to investigate the topotactic mechanism previously reported. The topotactic character of the reactions is confirmed and an approximate model for the crystal structure of $MoO_3 \cdot H_2O$ is proposed. Quantitative data about the relative amount of the existing phases, as a function of temperature, have been deduced from multiphase profile analysis. The anomalous behavior of the cell parameters of $MoO_3 \cdot H_2O$, at about 100°C, indicates the existence of a new phase transition. The evolution of the crystallite size of MoO_3 has also been obtained from the broadening of Bragg reflections at high temperature. The preferred direction of growth is along [021]*.

Introduction

Among the various molybdic acids mentioned in the literature, two compounds with formulae $MoO_3 \cdot 2H_2O$ and $MoO_3 \cdot H_2O$ (yellow and white monohydrated forms) are definite phases and have been extensively studied by X-ray single crystal diffraction (*1–6*) and NMR (*7*). The tungsten oxides $WO_3 \cdot 2H_2O$, $WO_3 \cdot H_2O$ and WO_3 have been closely compared with the corresponding Mo oxides; W and Mo hydrated oxides have been reported as isotypic (*1, 2*). The crystal structures of $WO_3 \cdot H_2O$ and WO_3 are described in (*8, 9*) respectively. In the case of the Mo oxides studied in this paper, the structure of the dihydrate (*3, 4*) and the white form of the monohydrate (*5, 6*) have been accurately determined and a structural model for the yellow form of the monohydrate has been proposed (*2*) on the basis of the topotactic nature of the dehydration reaction $MoO_3 \cdot 2H_2O \rightarrow MoO_3 \cdot H_2O \rightarrow MoO_3$. The 2D structure of the dihydrate is built from slightly distorted layers of corner sharing $MoO_5(H_2O)$ octahedra; these layers are stacked along the *b* axis and connected by interlayer water molecules. The first step of the dehydration in air corresponds to the removal of the interlayer water molecules from the dihydrate and leads to $MoO_3 \cdot H_2O$ which, in the second step, dehydrates to MoO_3. The structural changes during the dehydration process are schematized, following Ref. (*2*), in Fig. 1. The relationship between the lattices of all three compounds has been carefully determined by single crystal X-ray photographs (*2*). The dehydration to MoO_3 also takes place in a few hours at room temperature under a vacuum of about 10^{-4} Torr (*2*), but is then believed to occur continuously. Studies on the mechanism of solid state reactions are largely

¶ On leave from Institut de Physique, Université de Constantine, Algérie.

§ Present address: Laboratoire Léon Brillouin (CEA-CNRS) CE de Saclay, 91191 Gif sur Yvette Cedex, France.

0022-4596/93 $5.00

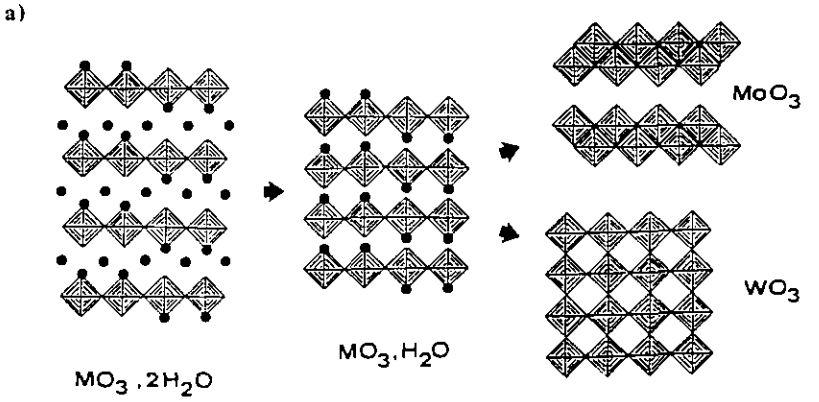

b) $MoO_3.2H_2O$ *(3)*

$a_2 = 10.476$ Å
$b_2 = 13.822$ Å
$c_2 = 10.606$ Å
$\beta = 91.62°$
$P2_1/n$

$MoO_3.H_2O$ *(2)*

$a_1 = 7.55$ Å
$b_1 = 10.69$ Å
$c_1 = 7.28$ Å
$\beta = 91°$
$P2_1/c$

MoO_3 *(13)*

$a_0 = 3.96$ Å
$b_0 = 13.86$ Å
$c_0 = 3.70$ Å

Pbnm

$a_1 = 1/2(a_2 - c_2)$ $\quad a_0 = 1/2\ a_1$
$c_1 = 1/2(a_2 + c_2)$ $\quad c_0 = 1/2\ c_1$

$WO_3.H_2O$ *(8)*

$a_O = 5.249$ Å
$b_O = 10.711$ Å
$c_O = 5.133$ Å

Pmnb

$MoO_3.H_2O$ *(this work)*

$a_M = 7.548$ Å
$b_M = 10.712$ Å
$c_M = 7.237$ Å
$\beta = 90.77°$
$P2_1/c$

$a_M = a_O + c_O$
$c_M = a_O - c_O$

FIG. 1. Scheme of the dehydration process $MoO_3 \cdot 2H_2O \rightarrow MoO_3 \cdot H_2O \rightarrow MoO_3$. The cell parameters of the different phases as well as the relations between the *a* and *c* parameters defining the topotactic character of the dehydration reactions, are indicated. The reduced two-dimensional cell to which we refer in the text corresponds to the cell of MoO_3.

based on single crystal studies by X-ray or electron diffraction; this approach is indeed needed to establish unambiguously the orientation relationship between parent phases involved in the transformation. Unfortunately such experiments do not bring any information about the kinetics of the process and, when kinetic data become available, e.g., through calorimetric or TGA (thermogravimetric analysis) investigation, they cannot usually be easily correlated with the diffraction data (for instance, because of the large differences of sample environment which may strongly influence the transfor-

mation itself). Experience gained during the recent years in real-time neutron diffraction at PSD (Position Sensitive Detectors)-equipped powder diffractometers has shown that thermodiffractometry (*10*) is a fast and powerful method to obtain in a single experiment both structural and kinetics information on solid state transformations, thus supplementing more conventional techniques. This is especially true in case of reactions involving the evolution of protonated species where changes in the incoherent background can be used to monitor the sample composition. In the present work, a thermodiffractometric study was carried out in order to investigate the topotactic dehydration which leads from the hydrate $MoO_3 \cdot 2H_2O$ to the oxide MoO_3.

Experimental Procedure and Data Analysis

$MoO_3 \cdot 2H_2O$ was prepared according to the Freedman method (*11*). An amount of 50 g of $Na_2MoO_4 \cdot 2H_2O$ was dissolved in 100 ml of water. The solution was added to 300 ml of 5 *N* HNO_3 at room temperature. Precipitation of the yellow $MoO_3 \cdot 2H_2O$ began within two days but the solution was allowed to complete precipitation for a few weeks (from 3 to 5). The precipitate was centrifuged and washed with 100 ml of 4 *N* HNO_3 and then with water. After five repeated centrifugations and washings in order to eliminate any sodium impurity, the precipitate was air-dried at room temperature.

The thermodiffractometry experiment was carried out on the high flux diffractometer D1B equipped with a PSD detector. The wavelength used was $\lambda = 2.52$Å; the sample (powdered $MoO_3 \cdot 2H_2O$ in a vanadium cylinder of $h = 50$ mm, $d = 10$ mm) was heated in a furnace, under a primary vacuum of about 10^{-3} Torr, in the range RT to 400°C at a rate of 20°C/h. The diffraction patterns were extracted every 3 min; the temperature change was ≈1°C per pattern.

All the 359 diffraction patterns collected were analyzed using the programs of the STRAP (*12*) package. Two kinds of refinement were carried out:

(1) The evolution with temperature of the peak positions, FWHM, integrated intensities, and shape parameters can be obtained using a numerical fit of pseudo-Voigt functions to several independent reflections for selected zones of the diffraction patterns. These parameters are necessary to calculate the crystallite size as a function of temperature.

(2) For the analysis of the full profile, the Rietveld method (*13*) was used. In the case of $MoO_3 \cdot 2H_2O$ the structural parameters were taken from (*3*) and kept fixed during the refinements; only the "profile parameters," i.e., cell parameter, background, and scale factors, were varied. The same method was applied to the patterns of MoO_3; the structural parameters were taken from (*14*). In the case of $MoO_3 \cdot H_2O$, we have deduced an approximate model of the structure which was precise enough to be introduced in the refinement procedure. With this procedure, an overall view of the evolution of cell parameters and the relative amount of each present phase can be obtained.

Results

Figure 2 shows a 3D plot of the diffraction pattern corresponding to the dehydration reactions $MoO_3 \cdot 2H_2O \rightarrow MoO_3 \cdot H_2O \rightarrow MoO_3$ in the temperature range RT to 400°C. The first peaks of the monohydrated phase appear at $T \approx 60$°C while the $MoO_3 \cdot 2H_2O$ phase does not vanish before $T \approx 80$°C. The dehydration leads to MoO_3 oxide which appears at about 150°C. The dependence of the incoherent background on the total amount of hydrogen in the sample can be observed. From the evolution of the background with the temperature, the existence of two stages in the dehydration process is clearly seen.

Günter (*2*) has already reported the two

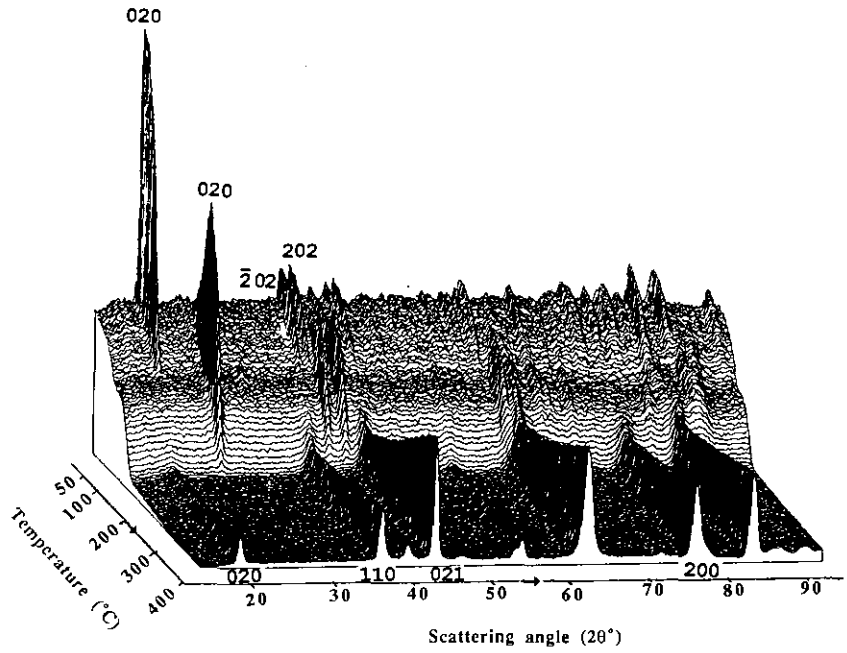

FIG. 2. Three-dimensional plot of the neutron diffraction patterns of the dehydration process $MoO_3 \cdot 2H_2O \rightarrow MoO_3 \cdot H_2O \rightarrow MoO_3$.

steps of dehydration corresponding to the two topotactic reactions. Figure 1 contains room temperature values of the lattice constants for the three compounds and the proposed structural scheme of the dehydration process (*2*). This figure points out the topotactic character of the reactions and the analogy between the three crystal structures. Regardless of the *b* axis (which is, in all cases, perpendicular to the MoO_6 sheets) a close relationship exists between the *a* and *c* axes of the three cells; the relations between the *a* and *c* axes are also given. As stated above, tungsten and molybdenum dihydrates are isotypic (*2, 15*) while the final oxides show two different arrangements for the octahedral MO_6 network (*14, 16, 17*). Günter has proposed a crystal structure model for $MoO_3 \cdot H_2O$ deduced from the topotactic character of the dehydration from $MoO_3 \cdot 2H_2O$ with the arrangement for the water molecules represented in Fig. 1. We have confirmed the general trends of Günter's results, but we found that the crystal structure of $MoO_3 \cdot H_2O$ seems to be just a monoclinic distortion of the $WO_3 \cdot H_2O$ (tungstite) structure described in (*8*) with identical arrangement of water molecules. In Fig. 1 we also give the relation between the orthorhombic cell of tungstite and the monoclinic cell of $MoO_3 \cdot H_2O$.

Our work has allowed us to give further details on the topotactic mechanism of the dehydration reactions. On the other hand, from the high temperature part of the experiment, we have obtained the crystallite size evolution of MoO_3 as a function of temperature. This new information leads to a deeper insight into the crystal growth process of MoO_3 in the annealing conditions of our experiment.

Crystal Structure of $MoO_3 \cdot H_2O$

The calculation of the neutron powder diffraction pattern of a hypothetical $MoO_3 \cdot H_2O$ having the same structure as tungstite, and using the crystallographic parameters from (*8*), confirms the close relationship be-

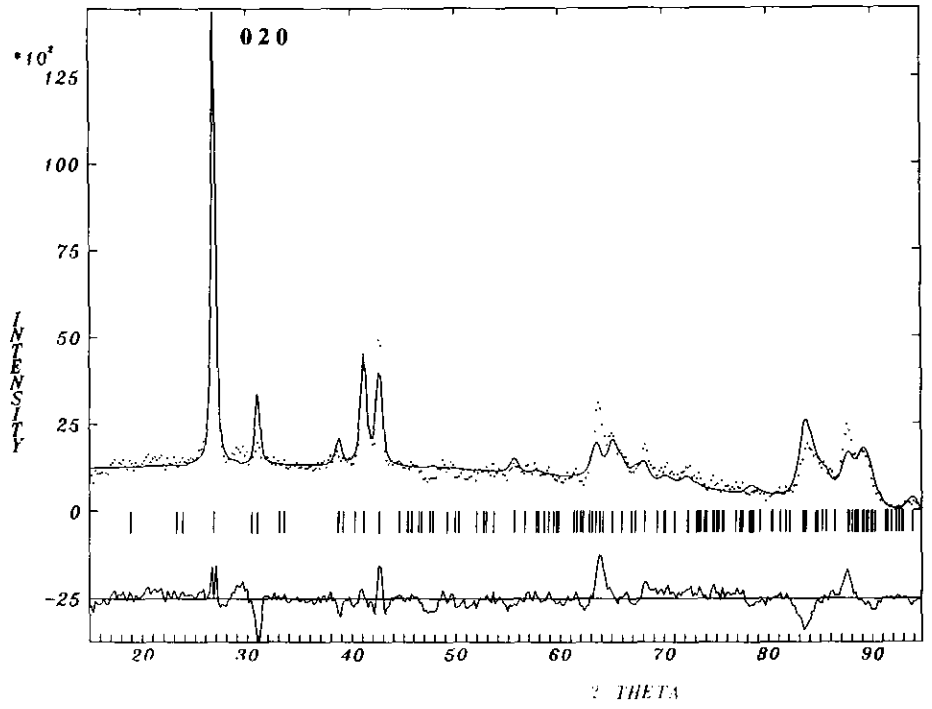

FIG. 3. Observed and calculated neutron powder diffraction pattern of $MoO_3 \cdot H_2O$.

tween the crystal structures of tungstite and $MoO_3 \cdot H_2O$. Regardless of the peak positions (tungstite is orthorhombic and $MoO_3 \cdot H_2O$ is monoclinic), the distribution of the peak intensities in the calculated pattern is very close to the observed one. We have determined the new atomic positions in $MoO_3 \cdot H_2O$, taking into account the monoclinic symmetry, from the relation between the orthorhombic cell of tungstite and the monoclinic cell of $MoO_3 \cdot H_2O$ (see Fig. 1). The deduced space group of $MoO_3 \cdot H_2O$ was $P2_1/c$.

Our experimental conditions were such that the full refinement of the structure could not be realized (too many parameters and small angular range of the diffraction patterns); however, this model provides good enough results to be considered as a good approximation to the real structure. Figure 3 shows an observed and calculated powder pattern of this phase corresponding to a temperature of about 90°C.

The isomorphism between tungstite and $MoO_3 \cdot H_2O$ implies that (at the same time as the disappearance of the interlayer water molecules from $MoO_3 \cdot 2H_2O$) the perovskite-like sheets not only collapse along the b axis, but also undergo a cooperative shift of vector $[\frac{1}{4}\ 0\ \frac{1}{4}]_{Di}$ ($[\frac{1}{2}\ 0\ 0]_{Mono}$) between each two consecutive layers. Figure 4 is a view of the structure; it can be seen that the MoO_6 octahedra are stacked in sheets (at $y = \frac{1}{4}$ and $\frac{3}{4}$) sharing four corners in the equatorial plane while water oxygen atoms alternate on the axial corners along [100] and [001] directions. All the sheets are linked by hydrogen bonds issued from H(1) and H(2) of the water oxygen O(1) to two O(2) atoms belonging to two octahedra of another sheet. These bonds extend in the [101] direction.

This structural model does not agree with the scheme proposed by Günter (*2*) and presented in Fig. 1.

Topotactic Reactions

In order to confirm the topotactic character of the reactions we have examined the

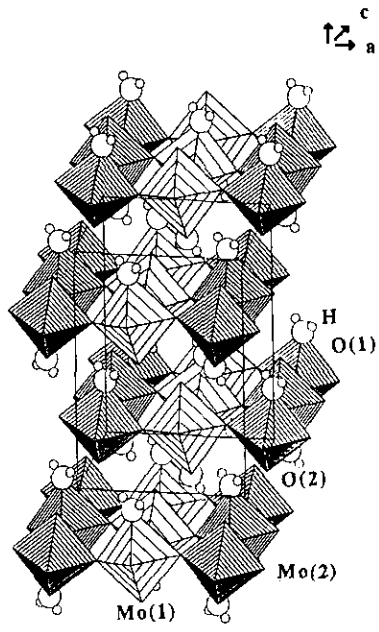

FIG. 4. Polyhedral representation of the $MoO_3 \cdot H_2O$ structure. The Mo(1) octahedra are less shaded than the Mo(2) ones.

evolution with the temperature of the volume per unit formula of the three oxides, which are represented in Fig. 5. The loss of one water molecule in the reaction $MoO_3 \cdot 2H_2O \rightarrow MoO_3 \cdot H_2O$ implies a volume reduction of about 25 Å^3; in the same way, the disappearance of the second water molecule (reaction: $MoO_3 \cdot H_2O \rightarrow MoO_3$) gives rise to the same volume reduction.

Making use of the relationships between the cell parameters of the three phases in the *ac* plane (see Fig. 1) it is instructive to represent the reduced cell parameters (equivalent to the *a*–*c* unit cell of MoO_3) a_r and c_r as a function of temperature. Figure 6 is an illustration of a_r and c_r parameter evolution versus temperature. Both parameters of dihydrate and oxide show a smooth monotonic evolution. In the oxide, they are nearly constant. In the dihydrate, while a_r slightly increases, c_r decreases at a comparable rate. On the contrary, in the case of the monohydrate a structural phase transition occurs: a_r and c_r vary with an opposite slope during the coexistence with the dihydrate and they undergo significant changes in opposite directions in a temperature range of 15°C above and below 103°C, which roughly corresponds to the whole disappearance of the dihydrated phase.

The effect on the peak positions of the cell parameter changes in $MoO_3 \cdot H_2O$ is particularly remarkable for the (210) reflection (see Fig. 2). We shall discuss below the possible origin of this structural phase transition.

Crystallite Size Evolution in MoO_3

The average crystallite sizes, in different directions normal to (*hkl*) planes, were calculated for MoO_3 from the profile parameters of selected reflections: five peaks were used to carry out this analysis. We have not tried to separate the strain component contribution to the peak broadening because only one order of (*hkl*) plane is available in the collected 2θ range. It is worth mentioning that, in single line analysis, the Cauchyian and Gaussian components are usually attributed to size and strain broadening, respectively (*18*). We consider this assumption to be too simple and we prefer to use the full integral breadth as a parameter characterizing the "apparent size" of the crystallites.

Our "crystallite size" corresponds, in fact, to an apparent size that is not only related to size effects. However, we consider that the main cause of broadening is the small crystallite size at the beginning of the formation of MoO_3. In any case the "apparent crystallite size" is a good parameter characterizing the crystal growth during the annealing treatment.

The pseudo-Voigt function was used to describe the peak shape (for a detailed description of this function and the shape parameters involved, see (*18*) and references therein). The most important parameter is the integral breadth β of the diffraction profile, which gives an indication of the average crystallite size normal to the reflecting planes (*hkl*). We call this crystallite/domain

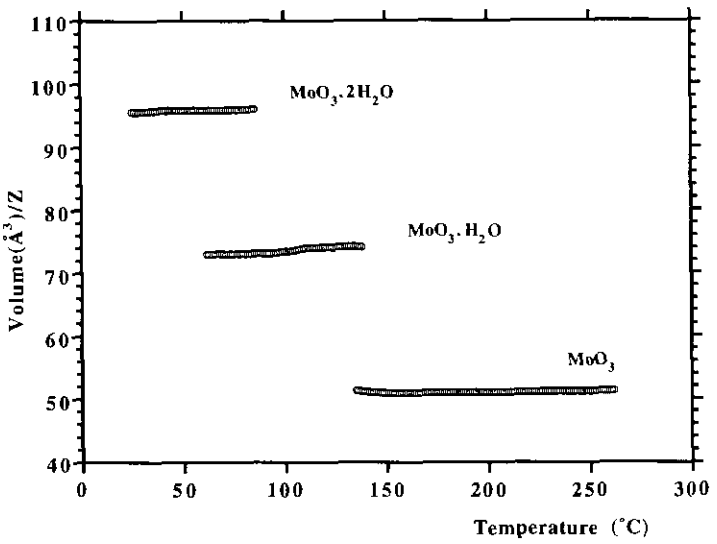

FIG. 5. Evolution of the volume per formula unit as a function of temperature of the three phases $MoO_3 \cdot 2H_2O$, $MoO_3 \cdot H_2O$, and MoO_3.

size parameter $\langle D \rangle_{app}$ and it is given by Scherrer's formula:

$$\langle D \rangle_{app} = \lambda / \beta \cos\theta.$$

The integral breadth of a unit area normalized pseudo-Voigt function is

$$\beta_{pv} = \int I(2\theta) d(2\theta) / I_{max} = w/[\eta/\pi + (1 - \eta)\sqrt{\ln 2/\pi}],$$

which is easily obtained from the fitted $2w$ and η parameters. In order to determine β from the peak profile one has to take into

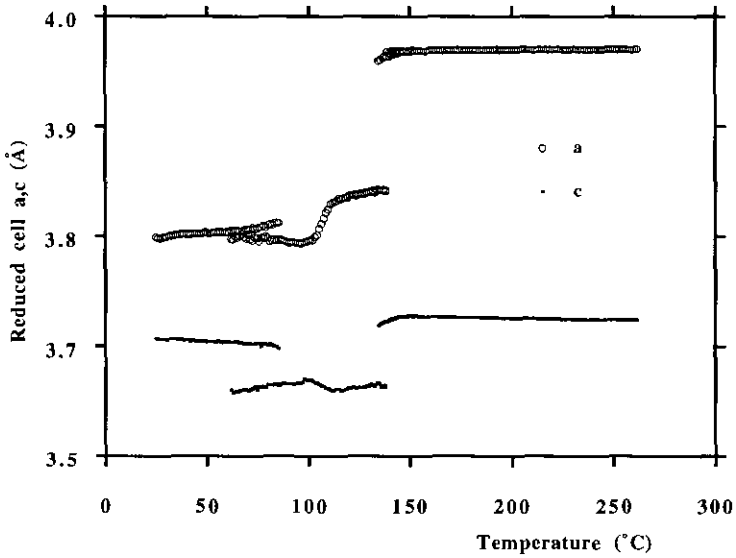

FIG. 6. Reduced cell parameters a_r and c_r as a function of temperature for the three phases.

account that the observed profile is the convolution of the intrinsic peak profile with the instrumental resolution function; this latter describes the peaks of a sample not affected by size and strain broadening.

As pointed out by Langford (*19*), if the peak shape is considered to be Voigtian, to correct for instrumental resolution we can use the formulae

$$(\beta_G^f)^2 = (\beta_G^h)^2 - (\beta_G^g)^2,$$
$$(\beta_C^f) = (\beta_C^h) - (\beta_C^g),$$

where the superscripts h and g stand for observed peak and instrumental profile, respectively, and f corresponds to the intrinsic diffraction profile.

We have obtained the Cauchyian and Gaussian components of the integral breadth as a function of the ratio $2w/\beta$ by using the formula given by de Keijser *et al.* (*20*).

The instrumental peak shape of D1B is gaussian. By fitting the peaks of a well crystallized material, YIG in our case, in the angular range 28–134.8 (°2θ), we have obtained the values of $(2w_G^g)$ = FWHM (full width at half maximum) as a function of 2θ angle. These values have been fitted to the Cagliotti–Paoletti–Ricci functional form:

$$(2w_G^g)^2 = U \tan^2\theta + V \tan\theta + W.$$

The values obtained for U, V, and W were $U = 1.309\ (17)$, $V = -0.744\ (31)$, $W = 0.238\ (12)$. Using the above formula to correct the measured integral breadths, we have synthesized the instrumental corrected integral breadth of the peaks and used this parameter through Scherrer's equation as a measure of the apparent crystallite size.

The apparent size increases in preferred directions. Indeed, after the peak profiles as a function of the temperature were sequentially refined, a program was made to determine the approximate crystallite size perpendicularly to the (*hkl*) planes. The results are put together as in Fig. 7. On this figure it is clear that the preferred direction of crystal growth is along [021]*. At the early stages of the formation of MoO_3, the crystallites have a marked anisotropy: the mean diameter perpendicular to the MoO_3 (010)-sheets is only about 50 Å, while it is about three times greater in the direction perpendicular to the (001) planes.

Discussion

The topotactic character of dehydration reactions in molybdenum oxides, formerly reported, is confirmed through a thermodiffractometry experiment (Fig. 2). The powder patterns obtained are composed of parts in which only one phase exists (dihydrate, monohydrate, or oxide) separated by diagrams showing the coexistence of two phases. The formation of the crystallites of each new phase is clearly detected by the presence of the extra Bragg reflections which first increase and then vanish when the crystallites of their phase disappear. This means that the dehydration reactions seem to begin in a part of the sample volume and stretch through the whole volume to crystallize the new phase. The most plausible mechanism is that water molecules in a crystallite of a hydrated phase are lost through the crystal faces not parallel to (010). As soon as the regions near the faces lose their water molecules, these are replaced with water molecules from the internal regions of the grain; in this way the less hydrated phase nucleates at the interior of the crystallites. The fact that there is no broadening of the $MoO_3 \cdot H_2O$ reflections can be related to a much softer dehydration process from $MoO_3 \cdot 2H_2O$ than in the case of MoO_3 formation.

Crystal structures of the dihydrated and anhydrous phases were previously known. We have proposed a model for the crystal structure of $MoO_3 \cdot H_2O$, deduced from the atomic arrangement of $WO_3 \cdot H_2O$; the representation of the structure in Fig. 4 clearly shows the water oxygen alternating on the axial corners of the octahedra along the [101] direction. As stated above, the arrangement of water molecules implies that

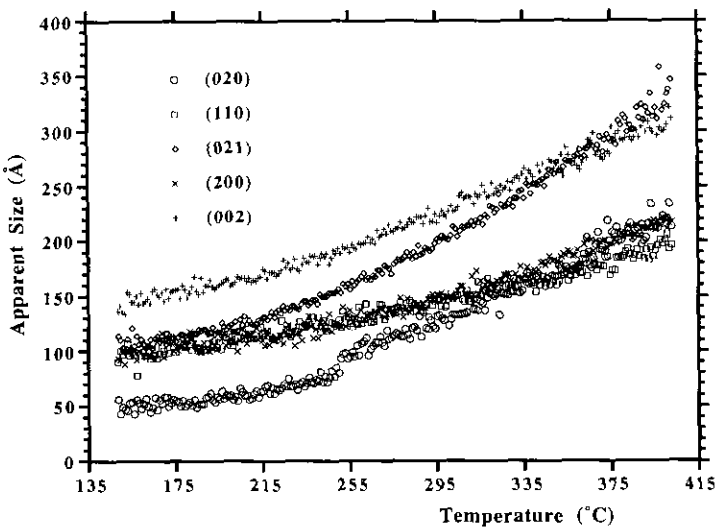

FIG. 7. Apparent crystallite size of MoO_3 in different directions as a function of temperature.

the dehydration reaction is not simply a removal of the water molecules layers followed by a collapse diminishing the distance between the MoO_6 octahedra sheets.

The particular ordering of Mo-bonded water molecules proposed by Günter (similar to $MoO_3 \cdot 2H_2O$) cannot be described in $P2_1/c$ with the unit cell proposed by him. In this space group we have the possibility to delocalize statistically the H atoms around the two axial oxygen atoms of each octahedron. However, the calculation does not improve the agreement between the observed and calculated powder patterns enough. Since better results concerning the crystal structure of $MoO_3 \cdot H_2O$ could not be obtained, due to the limited angular range of the PSD diffractometer, deeper discussions about this structure are not justified. Nevertheless it can be seen that the atomic arrangements of $MoO_3 \cdot H_2O$ and $WO_3 \cdot H_2O$ are similar.

In Fig. 8 we show the evolution as a function of temperature of the two most intense reflections belonging to the hydrated phases. No integrated intensity of a reflection corresponding to MoO_3 is represented, because at the earlier stage of the second dehydration reaction, the peaks of the oxide are very broad and the accuracy of their integrated intensity is lower than in the other phases.

The intensities are normalized to 100% for their maximum value, and represent the relative fraction of the respective phase: $x_{Di} \approx I(020)_{Di}$, $x_{Mono} \approx I\ (020)_{Mono}$. For the temperature range where the two hydrates coexist, the relation $x_{Di} + x_{Mono} = 100$ is satisfied within experimental error. The shape of the evolution curve for the fraction of $MoO_3 \cdot H_2O$ shows the typical sigmoid characteristic of a nucleation and growth process.

As noticed above, there is anomalous behavior of cell parameters at about 103°C for $MoO_3 \cdot H_2O$; this is also visible in the plot (Fig. 8) of the integrated intensity of the $(020)_{Mono}$ reflection, as a kink around the quoted temperature. This is another signature of the above-mentioned structural phase transition.

The nature of this phase transition is not well understood at present. It is, perhaps, a phenomenon related to some ordering of water molecules or, alternatively, a kind of displacive transition related to mechanical

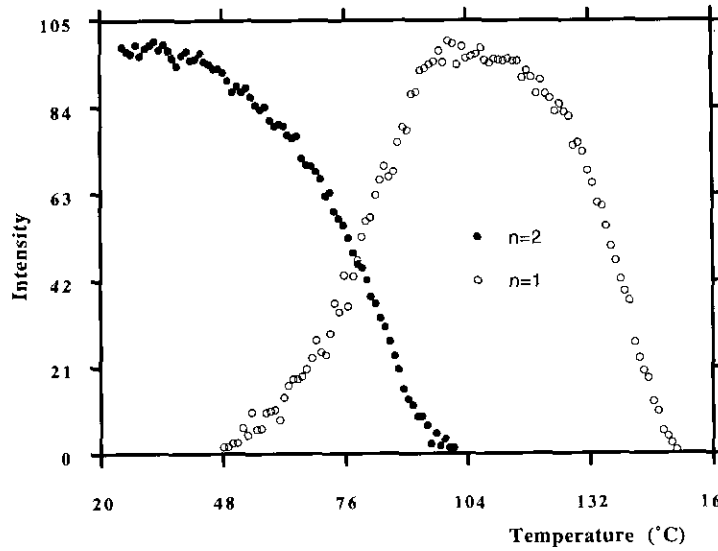

FIG. 8. Evolution of the phase proportion for $MoO_3 \cdot 2H_2O$ and $MoO_3 \cdot H_2O$ as a function of the temperature. These values have been obtained from the integrated intensities of the reflections $(020)_{Di}$ and $(200)_{Mono}$.

stress due to the coexistence of the two phases ($MoO_3 \cdot 2H_2O$ and $MoO_3 \cdot H_2O$) in the same grains.

A possible explanation of the observed changes can be found in the rearrangement of the water molecules at a second stage of the reaction. The first step of the dehydration reaction, $MoO_3 \cdot 2H_2O \rightarrow MoO_3 \cdot H_2O$, proceeds just by removing the interlayer water molecules of $MoO_3 \cdot 2H_2O$, which cost less in energy, accompanied by a mutual shift of the vector $[\frac{1}{4}\ 0\ \frac{1}{4}]_{Di}$ ($[\frac{1}{2}\ 0\ 0]_{Mono}$) of the perovskite-like sheets. In the second step, when the interlayer H_2O-molecules vanish, the rearrangement of the remaining H_2O-molecules takes place. The new arrangement of these water molecules around the axial corners is schematized in Fig. 9. This model implies that the structural transition has a diffusive character.

In spite of the similarities of tungsten and molybdenum monohydrates, their dehydration products are different. While WO_3 crystallizes in the perovskite ReO_3-type (*17*), α-MoO_3 is built of bilayers of Mo oxygen

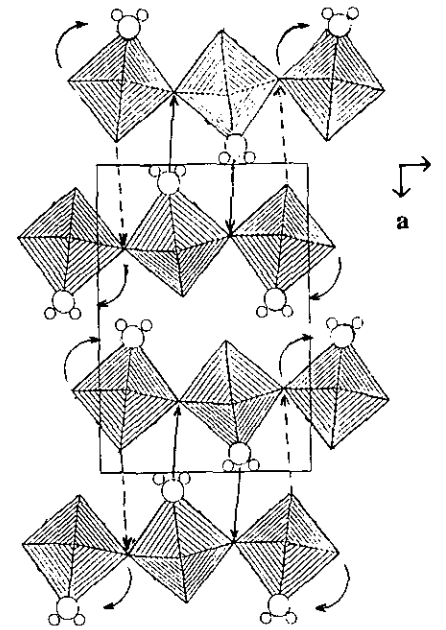

FIG. 9. Schematic mechanism of the dehydration process $MoO_3 \cdot H_2O \rightarrow MoO_3$.

octahedra sharing two edges (*14, 16*) arranged in an orthorhombic cell. The linkage of MoO_6 octahedra is similar to that found in the chains of $MoO_3 \cdot H_2O$ (white form) (*5, 6*). There are two other metastable polymorphs of MoO_3 (β-MoO_3 (*21–23*) and β'-MoO_3 (*24*)) which are different distortions of the ReO_3-type structure. It seems that MoO_3 can be stabilized in the ReO_3 structure by partially substituting Mo by W (*25*); in addition, it is worth noticing that the dehydration of the mixed oxides $Mo_{1-x}W_xO_3 \cdot H_2O$, which are isostructural to $MoO_3 \cdot H_2O$, leads to $Mo_{1-x}W_xO_3$ crystallizing in an ReO_3-like structure (*26*). According to (*26*), electron diffraction shows clearly the topotactic transformations of $WO_3 \cdot H_2O \rightarrow WO_3$ and $MoO_3 \cdot H_2O \rightarrow MoO_3$ in the ReO_3 structure which is transformed, in the case of the Mo compound, to the layered α-MoO_3 structure.

Under our experimental conditions the second dehydration reaction, $MoO_3 \cdot H_2O \rightarrow MoO_3$, seems to be more complex than the first one because of the final compact layer structure of MoO_3. However, a tentative schematic mechanism can be devised (Fig. 9): when the water molecules disappear the octahedra collapse following a displacement of the layers along the *a* axis (same crystallographic sites); then a jump of the equatorial oxygen atoms, those which are parallel to the *c* axis, is achieved according to the hypothetical rotation drawn in Fig. 9. In another way, this transformation could be explained as well on the basis of processes involving oriented nucleation and growth as explained in (*27*).

The reason for the different behavior of hydrated MoO_3 compared with tungsten oxides can be found in the existence of two nonequivalent crystallographic sites for Mo in the monoclinic $MoO_3 \cdot H_2O$, while in orthorhombic $WO_3 \cdot H_2O$ there is only one site for W, which behaves similarly during the dehydration giving rise to the ReO_3-type structure.

In order to solve the open questions stated by our work, a high resolution neutron powder diffraction experiment on deuterated samples should be carried out to complete the structure determination of $MoO_3 \cdot H_2O$ and determine the nature of the structural phase transition.

Acknowledgments

We are indebted to Jean Pannetier who has worked extensively in the preparation and development of the neutron diffraction experiment. His critical reading of the manuscript is also acknowledged.

References

1. I. Lindquist, *Acta Chem. Scand.* **4,** 650 (1950) and **10,** 1362 (1956).
2. J. R. Günter, *J. Solid State Chem.* **5,** 354 (1972).
3. B. Krebs, *Acta Crystallogr. Sect. B* **28,** 2222 (1972).
4. F. Cesbron and D. Ginderow, *Bull. Mineral.* **108,** 813 (1985).
5. V. Böschen and B. Krebs, *Acta Crystallogr. Sect. B* **30,** 1795 (1974).
6. H. R. Oswald, J. R. Günter, and E. Dubler, *J. Solid State Chem.* **13,** 330 (1985).
7. R. H. Jarman, P. G. Dickens, and R. C. T. Slade, *J. Solid State Chem.* **39,** 387 (1981).
8. J. T. Szymanski and A. C. Roberts, *Can. Mineral.* **22,** 681, (1984).
9. B. O. Loopstra and P. Boldrini, *Acta Crystallogr.* **21,** 158 (1966); see also B. O. Loopstra and H. M. Rietveld, *Acta Crystallogr. Sect. B* **25,** 1420 (1969).
10. J. Pannetier, *Chem. Script.* **26A,** 131 (1986).
11. M. L. Freedman, *J. Am. Chem. Soc.* **81,** 3834 (1959).
12. STRAP I.L.L., Internal Report 87RO14T, J. Rodríguez-Carvajal, M. Anne, and J. Pannetier (1987).
13. H. M. Rietveld, *Acta Crystallogr.* **22,** 151 (1967); the program used is a modified version of that described in *J. Appl. Crystallogr.* **15,** 430 (1982) by R. A. Young and D. B. Wiles.
14. G. Andersson and A. Magnéli, *Acta Chem. Scand.* **4,** 793 (1950).
15. M. L. Freedman and S. Leber, *J. Less-Common Met.* **7,** 427 (1964).
16. L. Kihlborg, *Ark. Kem.* **21,** 357 (1963).
17. S. Tanisaki, *J. Phys. Soc. Jpn.* **15,** 573 (1960).
18. Th. H. de Keijser, E. J. Mittemeijer, and H. C. F. Rozendaal, *J. Appl. Crystallogr.* **16,** 309 (1983).
19. J. I. Langford, *J. Appl. Crystallogr.* **11,** 10 (1978).
20. Th. H. de Keijser, J. I. Langford, E. J. Mittemeijer, and A. B. P. Vogels, *J. Appl. Crystallogr.* **15,** 308 (1982).
21. E. M. McCarron III, *J. Chem. Soc. Chem. Commun.* **4,** 336 (1986).

22. F. Harb, B. Gérand, G. Nowogrocki, and M. Figlarz, *C. R. Acad. Sci. Paris* **303** (II), 349 (1986).
23. G. Svensson and L. Kihlborg, *React. Solids* **3,** 33 (1987).
24. J. B. Parise, E. M. McCarron, A. W. Sleight, and E. Prince, *Mater. Sci. Forum* **27–28,** 85 (1988).
25. E. Salje, R. Gehlig, and K. Viswanathan, *J. Solid State Chem.* **25,** 239 (1978).
26. L. Ganapathi, A. Ramanan, J. Gopalakrishnan, and C. N. R. Rao, *J. Chem. Soc. Chem. Commun.* 62 (1986).
27. M. Figlarz, B. Gérand, A. Delahaye-Vidal, B. Dumont, F. Harb, A. Coucou, and F. Fievet, *Solid State Ionics* **43,** 143 (1990).